Generalized Likelihood Ratio Test for Modified Replacement Model in Hyperspectral Imaging Detection

François Vincent[a,*], Olivier Besson[a]

[a]*ISAE-SUPAERO, 10 Avenue Edouard Belin, 31055 Toulouse, France.*

Abstract

The replacement model, which assumes that the abundances sum up to one, is often advocated for subpixel target detection in hyperspectral imaging, and various detection schemes based on this model have been developed in the literature. However, in practical situations, this unitary constraint may be too strong due to possible attenuation of the target bidirectional reflectance distribution function, signature mismatches or impediments in the radiometric corrections. In this paper, we relax this unitary constraint and consider a modified replacement model. One step and two steps generalized likelihood ratio tests are developed for the proposed model and compared to standard solutions through numerical simulations. A real data experiment attests to the validity of the proposed approach.

Keywords: Hyperspectral, Detection, Subpixel, Replacement Model, GLRT, Kelly.

1. Introduction

An hyperspectral image is an extension of a standard three colors map to a spectrally more dense image, usually composed of hundreds of bands. This richer information allows to characterize or recognize the different materials present in a picture and hence hyperspectral imaging has encountered a large field of applications, ranging from remote sensing to medicine [1, 2, 3, 4, 5, 6, 7, 8].

When dealing with detection, two kinds of algorithms can be considered, namely anomaly detection where the target signature is unknown, and target detection where the target signature is known, usually from laboratory experiments. In this latter case, many algorithms have been developed in the literature, such as the Adaptive Matched Filter (AMF) [9], Kelly's GLRT [10], the Orthogonal Subspace Projection (OSP) [11], or the Adaptive Coherent/Cosine Estimator (ACE) [12], to cite a few. All these widely used algorithms are based on the so-called additive model which simply describes the observation data as the sum of a background nuisance plus a possible fraction of the known target signature. More recently, some of these algorithms have been extended to the more realistic replacement model [13, 14], where the target

*Corresponding author

Email addresses: francois.vincent@isae-supaero.fr (François Vincent), olivier.besson@isae-supaero.fr (Olivier Besson)

is supposed to replace an equivalent part of the background, see equation (1) below. The additive model can be viewed as a low target to background ratio approximation of the replacement model. In this more realistic model, a unitary constraint is enforced on the sum of the so-called abundances, corresponding to the proportion of each component, also called endmembers. However, this theoretical unitary constraint seems to be too restrictive in many practical applications where sources of uncertainty may question its validity.

The main reason of a possible mismatch is linked to the unknown aspect angle when considering large targets, such as vehicles for instance. This non-Lambertian target behaviour is well-known and can be modelled by a Bidirectional Reflectance Distribution Function (BRDF) when the aspect angles are known [15]. The consequence is a loss in the observed target abundance, compared to the laboratory measurements, that invalidates the unitary constraint. This effect has been observed on real data detection experiments where the target abundance is often under-estimated [16]. In this paper, we propose a Modified Replacement Model (MRM) which takes into account this possible BRDF attenuation due to the unknown attitude of the target with respect to the sensor. This model amounts to relax the unitary constraint on the abundances while still considering a background abundance attenuation when a target is present, unlike for the simple additive model. Hence, this MRM can be considered as a compromise between the replacement model, that seems too restrictive for real life applications and the standard additive model, that is oversimplified.

Moreover, while relaxing the unitary constraint, we also expect that the proposed detectors, adapted to the MRM, are also more robust to target signature mismatches than algorithms based on the strict replacement model. Indeed, in practice, there usually exists a spectral difference between the actual target signature and the presumed one. The principal reasons of these mismatches are a possible difference between the laboratory sensors and the experimental ones, non-complete atmospheric and sun illumination corrections, or simply an actual difference between the presumed target and the real one. In this case, as the background in the Pixel Under Test (PUT) is characterized using the nearby pixels, any target mismatch will also invalidate the assumed unitary constraint.

In this paper, we developed two Generalized Likelihood Ratio Tests (GLRT) for the MRM, namely the direct one-step GLRT and the two-steps GLRT, assuming that the background characteristics are known from secondary data. This last two-step GLRT is then the counterpart of the so-called Finite Target Matched Filter (FTMF) [13] for the MRM. Similarly, the one-step GLRT of the present paper, which we refer to as Sub-Pixel Adaptive DEtection (SPADE), is the counterpart of ACUTE [14]. The validity of these new detectors is assessed both on simulated and real data. The performance of these schemes on real data confirm the relevance of the proposed MRM.

The paper is organized as follows. We first describe the MRM and introduce the detection problem in section 2. The two kinds of GLRT are then derived in section 3 and section 4. These new detectors are compared to standard detectors both through numerical simulations in section 5, and real data in section 6. Finally concluding remarks end this paper in section 7.

2. Signal Model

The standard model in hyperspectral detection procedures, is the replacement model [17]

$$\mathbf{y} = \gamma\mathbf{t} + (1-\gamma)\mathbf{b} \tag{1}$$

where $\mathbf{y}$ represents the spectral vector of the Pixel Under Test (PUT), composed of N spectral samples, $\mathbf{t}$ represents the endmember we are looking for, $0 \leq \gamma \leq 1$ is the unknown abundance of the variety characterized by $\mathbf{t}$ also known as the fill factor, and $\mathbf{b}$ is the background spectral signature, assumed to be Gaussian, $\mathbf{b} \sim N(\boldsymbol{\mu}, \mathbf{R})$.

As stated in the introduction, the reflectance of a geometric target, such as a vehicle for instance, is subject to its unknown aspect angle with respect to the sensor. Thus, the observed target reflectance will possibly be affected by an unknown scaling factor δ, while the background abundance will remain linked to the real target masking surface in the pixel $(1-\gamma)$. Taking into account this target directional response, we consider the following **Modified Replacement Model** (MRM):

$$\mathbf{y} = \delta\gamma\mathbf{t} + (1-\gamma)\mathbf{b} \tag{2}$$

or, as both δ and γ are unknown, simply:

$$\mathbf{y} = \alpha\mathbf{t} + \beta\mathbf{b} \tag{3}$$

where both α and β are unknowns. It has to be noticed that as δ represents a sort of scaling factor for the presumed laboratory target spectrum due to a more grazing aspect angle, it will be usually lower than unity. Hence, the standard constraint on the sum of the total abundances is no more valid while using this MRM. Nevertheless, this model is not tantamount to considering a simplified additive model, because the noise abundance is supposed to change between the null hypothesis H_0 and the alternative hypothesis H_1, defined as

$$\begin{aligned} H_0 &: \mathbf{y} = \mathbf{b} \\ H_1 &: \mathbf{y} = \alpha\mathbf{t} + \beta\mathbf{b} \end{aligned} \tag{4}$$

As mentioned in the introduction, this model is also supposed to be able to manage possible mismatches in the target or background endmembers, because it relaxes the unitary constraint on the abundances.

3. Two-Steps GLRT

In this section, we will derive the GLRT associated with model (4), assuming that we have access to target-free data, namely secondary data, enabling the estimation of both the mean and the covariance

matrix of the background. Under the stated assumptions, the log-likelihood under H_1 is, up to additive and multiplicative constants,

$$L_1 = N\log(\beta^2) + \frac{(\mathbf{y} - \alpha\mathbf{t} - \beta\boldsymbol{\mu})^T\mathbf{R}^{-1}(\mathbf{y} - \alpha\mathbf{t} - \beta\boldsymbol{\mu})}{\beta^2}$$

or equivalently

$$L_1 = N\log(\beta^2) + \frac{(\mathbf{y}_b - \alpha\mathbf{t}_b - \beta\boldsymbol{\mu}_b)^T(\mathbf{y}_b - \alpha\mathbf{t}_b - \beta\boldsymbol{\mu}_b)}{\beta^2}$$

where $\mathbf{y}_b = \mathbf{R}^{-\frac{1}{2}}\mathbf{y}$, $\mathbf{t}_b = \mathbf{R}^{-\frac{1}{2}}\mathbf{t}$ and $\boldsymbol{\mu}_b = \mathbf{R}^{-\frac{1}{2}}\boldsymbol{\mu}$ are respectively the whitened data, target endmember and background mean. The Maximum Likelihood (ML) estimate of α is shown to be

$$\hat{\alpha} = \frac{\mathbf{t}_b^T(\mathbf{y}_b - \beta\boldsymbol{\mu}_b)}{\mathbf{t}_b^T\mathbf{t}_b} \tag{5}$$

so that the compressed log-likelihood under H_1 becomes

$$\max_{\alpha} L_1 = N\log(\beta^2) + \frac{(\mathbf{y}_b - \beta\boldsymbol{\mu}_b)^T\mathbf{P}^{\perp}(\mathbf{y}_b - \beta\boldsymbol{\mu}_b)}{\beta^2}$$

with $\mathbf{P}^{\perp} = \mathbf{I} - \mathbf{P}$ where $\mathbf{P} = \mathbf{t}_b(\mathbf{t}_b^T\mathbf{t}_b)^{-1}\mathbf{t}_b^T$. Differentiating with respect to β conducts to

$$N\beta^2 = \mathbf{y}_b^T\mathbf{P}^{\perp}(\mathbf{y}_b - \beta\boldsymbol{\mu}_b)$$

so that the ML estimate of β is the solution to the following second order equation:

$$N\beta^2 + \mathbf{y}_b^T\mathbf{P}^{\perp}\boldsymbol{\mu}_b\beta - \mathbf{y}_b^T\mathbf{P}^{\perp}\mathbf{y}_b = 0 \tag{6}$$

In order to obtain a positive value for β, the only valid solution is

$$\hat{\beta} = \frac{-\mathbf{y}_b^T\mathbf{P}^{\perp}\boldsymbol{\mu}_b + \sqrt{(\mathbf{y}_b^T\mathbf{P}^{\perp}\boldsymbol{\mu}_b)^2 + 4N\mathbf{y}_b^T\mathbf{P}^{\perp}\mathbf{y}_b}}{2N}$$

Hence the GLRT writes

$$T_2 = -N\log(\hat{\beta}^2) + (\mathbf{y}_b - \boldsymbol{\mu}_b)^T(\mathbf{y}_b - \boldsymbol{\mu}_b) - \frac{(\mathbf{y}_b - \hat{\beta}\boldsymbol{\mu}_b)^T\mathbf{P}^{\perp}(\mathbf{y}_b - \hat{\beta}\boldsymbol{\mu}_b)}{\hat{\beta}^2}$$

We can notice that, when no background power variation is detected ($\hat{\beta} = 1$), the proposed detector is equal to the AMF $T_{AMF} = (\mathbf{y}_b - \boldsymbol{\mu}_b)^T\mathbf{P}(\mathbf{y}_b - \boldsymbol{\mu}_b)$ [9]. Using (6), we can also rewrite T_2 as follows

$$T_2 = N(1 - \log(\hat{\beta}^2)) + (\mathbf{y}_b - \boldsymbol{\mu}_b)^T(\mathbf{y}_b - \boldsymbol{\mu}_b) + \frac{\boldsymbol{\mu}_b^T\mathbf{P}^{\perp}\mathbf{y}_b}{\hat{\beta}} - \boldsymbol{\mu}_b^T\mathbf{P}^{\perp}\boldsymbol{\mu}_b$$

The two-steps GLRT is finally obtained by replacing $\boldsymbol{\mu}$ and $\mathbf{R}$ by their ML estimates obtained from secondary data.

4. One-Step GLRT (SPADE)

Following Kelly's approach [10], we now derive the direct (one-step) GLRT, i.e. considering that the background characteristics (mean and covariance matrix) are not a-priori known. Hence, we assume that we can access K secondary data $\mathbf{z}_k, k = 0..., (K-1)$, free from the target endmember $\mathbf{t}$ i.e. $\mathbf{z}_k \sim N(\boldsymbol{\mu}, \mathbf{R})$.

From the stated model, the likelihood function under H_0 is now

$$\begin{aligned} p_0 &= \frac{1}{\sqrt{(2\pi)^N |\mathbf{R}|}} e^{-\frac{1}{2}(\mathbf{y}-\boldsymbol{\mu})^T \mathbf{R}^{-1}(\mathbf{y}-\boldsymbol{\mu})} \times \prod_{k=0}^{K-1} \frac{1}{\sqrt{(2\pi)^N |\mathbf{R}|}} e^{-\frac{1}{2}(\mathbf{z}_k-\boldsymbol{\mu})^T \mathbf{R}^{-1}(\mathbf{z}_k-\boldsymbol{\mu})} \\ &= \frac{1}{[(2\pi)^N |\mathbf{R}|]^{\frac{K+1}{2}}} e^{-\frac{1}{2}\mathrm{Tr}\{\mathbf{R}^{-1}\boldsymbol{\Sigma}_0\}} \end{aligned}$$

where $\boldsymbol{\Sigma}_0 = \sum_{k=0}^{K-1}(\mathbf{z}_k - \boldsymbol{\mu})(\mathbf{z}_k - \boldsymbol{\mu})^T + (\mathbf{y} - \boldsymbol{\mu})(\mathbf{y} - \boldsymbol{\mu})^T$. The mean and covariance matrix which maximize this likelihood are shown to be respectively

$$\begin{aligned} \hat{\boldsymbol{\mu}}_0 &= \frac{K\bar{\mathbf{z}} + \mathbf{y}}{K+1} \\ \hat{\mathbf{R}}_0 &= \frac{1}{K+1}[\mathbf{Z}\mathbf{Z}^T + \mathbf{y}\mathbf{y}^T - (K+1)\hat{\boldsymbol{\mu}}_0\hat{\boldsymbol{\mu}}_0^T] \\ &= \frac{1}{K+1}[\mathbf{Z}\mathbf{Z}^T - K\bar{\mathbf{z}}\bar{\mathbf{z}}^T + \frac{K}{K+1}(\mathbf{y} - \bar{\mathbf{z}})(\mathbf{y} - \bar{\mathbf{z}})^T] \end{aligned}$$

where $\mathbf{Z} = \begin{bmatrix} \mathbf{z}_0 & \dots & \mathbf{z}_{K-1} \end{bmatrix}$, $\bar{\mathbf{z}} = \frac{1}{K}\mathbf{Z}\mathbf{1}$ and $\mathbf{1}$ is a column vector composed of ones. The compressed likelihood under H_0 becomes

$$\max_{\boldsymbol{\mu},\mathbf{R}} p_0 = \left[(2\pi e^{-1})^N |\hat{\mathbf{R}}_0|\right]^{\frac{-(K+1)}{2}}$$

Additionally, the likelihood under H_1 is

$$\begin{aligned} p_1 &= \frac{1}{\sqrt{(2\pi)^N |\beta^2\mathbf{R}|}} \times e^{-\frac{1}{2\beta^2}(\mathbf{y}-\alpha\mathbf{t}-\beta\boldsymbol{\mu})^T \mathbf{R}^{-1}(\mathbf{y}-\alpha\mathbf{t}-\beta\boldsymbol{\mu})} \times \prod_{k=0}^{K-1} \frac{1}{\sqrt{(2\pi)^N |\mathbf{R}|}} e^{-\frac{1}{2}(\mathbf{z}_k-\boldsymbol{\mu})^T \mathbf{R}^{-1}(\mathbf{z}_k-\boldsymbol{\mu})} \\ &= \frac{1}{\beta^N [(2\pi)^N |\mathbf{R}|]^{\frac{K+1}{2}}} e^{-\frac{1}{2}\mathrm{Tr}\{\mathbf{R}^{-1}\boldsymbol{\Sigma}_1\}} \end{aligned}$$

where $\boldsymbol{\Sigma}_1 = \sum_{k=0}^{K-1}(\mathbf{z}_k - \boldsymbol{\mu})(\mathbf{z}_k - \boldsymbol{\mu})^T + (\tilde{\mathbf{y}} - \boldsymbol{\mu})(\tilde{\mathbf{y}} - \boldsymbol{\mu})^T$ and $\tilde{\mathbf{y}} = \frac{\mathbf{y}-\alpha\mathbf{t}}{\beta}$. Hence, the mean and covariance matrix estimates become

$$\begin{aligned} \hat{\boldsymbol{\mu}}_1 &= \frac{K\bar{\mathbf{z}} + \tilde{\mathbf{y}}}{K+1} \\ \hat{\mathbf{R}}_1 &= \mathbf{Z}\mathbf{Z}^T - K\bar{\mathbf{z}}\bar{\mathbf{z}}^T + \frac{K}{K+1}(\tilde{\mathbf{y}} - \bar{\mathbf{z}})(\tilde{\mathbf{y}} - \bar{\mathbf{z}})^T \end{aligned}$$

and

$$\max_{\boldsymbol{\mu},\mathbf{R}} p_1 = \beta^{-N}\left[(2\pi e^{-1})^N |\hat{\mathbf{R}}_1|\right]^{\frac{-(K+1)}{2}}$$

Notice that $|\hat{\mathbf{R}}_1| = \frac{1}{(K+1)^N}|\mathbf{S}| \times [1 + \frac{K}{K+1}(\tilde{\mathbf{y}} - \bar{\mathbf{z}})^T\mathbf{S}^{-1}(\tilde{\mathbf{y}} - \bar{\mathbf{z}})]$ where $\mathbf{S} = \mathbf{Z}\mathbf{Z}^T - K\bar{\mathbf{z}}\bar{\mathbf{z}}^T$. Differentiating the compressed log-likelihood with respect to α yields

$$\frac{\partial\tilde{\mathbf{y}}}{\partial\alpha}\mathbf{S}^{-1}(\tilde{\mathbf{y}} - \bar{\mathbf{z}}) = 0$$

so that the ML estimate of α writes

$$\hat{\alpha} = \frac{\mathbf{t}^T\mathbf{S}^{-1}(\mathbf{y} - \beta\bar{\mathbf{z}})}{\mathbf{t}^T\mathbf{S}^{-1}\mathbf{t}} = \frac{\mathbf{t}_w^T(\mathbf{y}_w - \beta\bar{\mathbf{z}}_w)}{\mathbf{t}_w^T\mathbf{t}_w} \tag{7}$$

where $\mathbf{y}_w = \mathbf{S}^{-\frac{1}{2}}\mathbf{y}$, $\mathbf{t}_w = \mathbf{S}^{-\frac{1}{2}}\mathbf{t}$ and $\bar{\mathbf{z}}_w = \mathbf{S}^{-\frac{1}{2}}\bar{\mathbf{z}}$ are respectively the data, target endmember and secondary data mean, whitened by the estimated covariance matrix, namely $\mathbf{S}$ (up to the $(K+1)$ scaling factor). As

$$(\tilde{\mathbf{y}}(\hat{\alpha}) - \bar{\mathbf{z}})^T\mathbf{S}^{-1}(\tilde{\mathbf{y}}(\hat{\alpha}) - \bar{\mathbf{z}}) = \frac{1}{\beta^2}(\mathbf{y}_w - \beta\bar{\mathbf{z}}_w)^T\mathbf{P}^{\perp}(\mathbf{y}_w - \beta\bar{\mathbf{z}}_w)$$

with $\mathbf{P}^{\perp} = \mathbf{I} - \mathbf{t}_w(\mathbf{t}_w^T\mathbf{t}_w)^{-1}\mathbf{t}_w^T$, we obtain

$$\max_{\boldsymbol{\mu},\mathbf{R},\alpha} L_1 = \text{const.} - N\log(\beta) - \frac{K+1}{2}\log\left[1 + \frac{K}{K+1}\frac{(\mathbf{y}_w - \beta\bar{\mathbf{z}}_w)^T\mathbf{P}^{\perp}(\mathbf{y}_w - \beta\bar{\mathbf{z}}_w)}{\beta^2}\right]$$

Differentiating this last expression with respect to β yields

$$\frac{N}{\beta} = \frac{K}{\beta^3}\frac{\mathbf{y}_w^T\mathbf{P}^{\perp}(\mathbf{y}_w - \beta\bar{\mathbf{z}}_w)}{\left[1 + \frac{K}{K+1}\frac{(\mathbf{y}_w - \beta\bar{\mathbf{z}}_w)^T\mathbf{P}^{\perp}(\mathbf{y}_w - \beta\bar{\mathbf{z}}_w)}{\beta^2}\right]} \tag{8}$$

Hence we need to solve the following 2^{nd}-order equation

$$N(1 + \frac{K}{K+1}\bar{\mathbf{z}}_w^T\mathbf{P}^{\perp}\bar{\mathbf{z}}_w)\beta^2 + K(1 - \frac{2N}{K+1})\mathbf{y}_w^T\mathbf{P}^{\perp}\bar{\mathbf{z}}_w\beta - K(1 - \frac{N}{K+1})\mathbf{y}_w^T\mathbf{P}^{\perp}\mathbf{y}_w = 0$$

where the product of the two roots is shown to be negative since $K + 1 - N > 0$. Hence, the only valid solution corresponds to the positive root.

Furthermore, considering that $|\hat{\mathbf{R}}_0| = \frac{1}{(K+1)^N}|\mathbf{S}|[1 + \frac{K}{K+1}(\mathbf{y}_w - \bar{\mathbf{z}}_w)^T(\mathbf{y}_w - \bar{\mathbf{z}}_w)]$, the GLRT is shown to be

$$T_{SPADE} = \frac{|\hat{\mathbf{R}}_0|^{\frac{K+1}{2}}}{\hat{\beta}^N|\hat{\mathbf{R}}_1|^{\frac{K+1}{2}}} = \frac{\left[1 + \frac{K}{K+1}(\mathbf{y}_w - \bar{\mathbf{z}}_w)^T(\mathbf{y}_w - \bar{\mathbf{z}}_w)\right]^{\frac{K+1}{2}}}{\hat{\beta}^N\left[1 + \frac{K}{K+1}\frac{(\mathbf{y}_w - \hat{\beta}\bar{\mathbf{z}}_w)^T\mathbf{P}^{\perp}(\mathbf{y}_w - \hat{\beta}\bar{\mathbf{z}}_w)}{\hat{\beta}^2}\right]^{\frac{K+1}{2}}}$$

5. Numerical simulations

In order to asses the validity of these new detectors, we consider an hyperspectral image composed of $N = 32$ spectral bands. The background comprises 5 random endemembers plus a -10 dB white Gaussian noise floor. A possible target, associated with a fill factor $\alpha = 0.2$ is also generated with a random spectral signature. For all simulations, we assume that $K = 10N$ in order to avoid a bad conditioning of the sample covariance matrix. We compare the two proposed GLRT, namely SPADE (section 4) and the

modified FTMF (section 3) with the standard AMF drawn from the additive model, and the two GLRT developed in the unitary constraint case, namely FTMF and ACUTE [14]. Figures 1, 2 and 3 present the Receiver Operating Characteristics (ROC), obtained from 10^5 Monte-Carlo simulations, respectively for targets BRDF attenuations equal to $\delta = 1$, $\delta = 0.7$ and $\delta = 0.5$.

We can observe that when the unitary constraint holds ($\delta = 1$), it is preferable to use the two detectors that perfectly fit the replacement model, namely FTMF and ACUTE detectors. The two detectors proposed in this paper exhibit a loss in this case, but still perform better than the standard AMF, which does not consider any background power variation between H_0 and H_1. When the unitary constraint on the abundances is no more satisfied, the two proposed GLRT keep the same performance whereas the other detectors degrade. Thereby, when the actual target amplitude decreases of more than 30% from the presumed one ($\delta < 0.7$), the proposed detectors are the best alternatives. A noticeable performance improvement can then be obtained. For instance, when $\delta = 0.5$, the gain is more than one decade in terms of P_{fa} for a given P_d. Moreover, we can see that the performance of FTMF and ACUTE are the same. Indeed, they are based on the same model, namely the exact replacement model and only differ in the way they solve the detection problem. FTMF is a two-steps procedure whereas ACUTE is a one-step algorithm. This last procedure is recognized to be more robust to a small number of training samples, but since $K = 10 \times N$ here this advantage is not visible. However, this benefit is slightly noticeable between the one-step and two-steps versions of the MRM GLRT, namely SPADE and the modified FTMF proposed in this paper.

6. Real Data Assessment

The two detectors proposed in this paper aim at improving the robustness on real data, assuming that the unitary constraint of the replacement model does possibly not hold. The goal of this last section is to test our proposed schemes against a real detection benchmark. We choose the "airborne Viareggio 2013 trial" open data to assess the different algorithms [18]. This benchmarking hyperspectral detection campaign took place in Viareggio (Italy), in May 2013, where an aircraft flying at 1200 meters heigh, acquired 3 $[450 \times 375]$ pixels maps of the same area. Two of them corresponding to a cloudy day, whereas the last one was acquired during a clear weather. Each hyperspectral pixel corresponds a $N = 511$ uniform sampling of the Visible Near InfraRed (VINR) band $(400 - 1000nm)$. The corresponding spatial resolution is about 0.6 meters.

Different kinds of vehicles as well as coloured panel served as known targets. For each of these targets, a spectral signature, obtained from ground spectroradiometer measurements, is available as well as the ground truth position. Moreover, a black and a white cover serving as calibration targets were also deployed. Indeed, these two calibrated targets, can be used to convert the raw Digital Numbers (DN) measurements into a reflectance map, using, for instance the ELM procedure.

In this paper, we consider the clear sky image, represented in Fig. (4). The scene is composed of

parking lots, roads, buildings, sports fields and pine woods. The black and white calibration panel are clearly visible, in positions $[70, 330]$ and $[250, 150]$ respectively. Among the 4 target vehicles, two are easily detectable, namely V1 and V4, as there signatures are far from the background subspace. These targets correspond to the blue car that can be seen in position $[250, 200]$, and a white vehicle covered with a red sheet in position $[130, 280]$. The two other vehicles, namely V5 and V6 are more difficult to detect because of signatures closer to the background subspace. We will focus on these more challenging targets (cf. Fig. 4).

The first step of the processing aims at converting the raw measurements into a reflectance map, for which the unitary constraint on the abundances is supposed to be verified. To this end, we use the ELM technique, considering the black and white calibration panels.

Once again, we compare the performances of the two proposed detectors with the AMF and with the two GLRT matching the replacement model exactly, namely FTMF and ACUTE. The performance is evaluated in counting the number of pixels where the detector output is larger than the output for the actual target position. This score corresponds to a false alarm number with an optimal threshold. For this real data experiment, we have chosen a guard window size of 9×9 pixels, considering the maximum extend of the vehicles used as targets, and a covariance estimation window of size 15×15, leading to $K = 4.5N$ secondary pixels. This comparison is performed for the V5 and V6 vehicles and is available on table 1.

On these two real targets, we can see that the performance of the two-steps MRM algorithm is roughly the same as its replacement-model counterpart, namely the FTMF, as it is better on V6 but worse on V5. On the other hand, the one-step MRM algorithm (SPADE) exhibits better or the same results as its replacement-model counterpart, namely ACUTE, for the two targets.

These real data results tend to confirm the relevance of the proposed MRM, relaxing the unitary constraint on the abundances, and leading to possibly better results in practice. It has to be noticed the good behaviour of the simple AMF compared to the FTMF, especially for the V6 target, suggesting again, that the unitary constraint may not hold. Indeed, using a simple additive model produces better results than considering the replacement one. The proposed MRM is somehow midway between the simple additive model and the too constrained replacement one.

7. Conclusions

In this paper we considered the detection problem of a target whose spectral signature is known up to a scaling factor, in an hyperspectral image. This situation occurs, for instance when the unknown aspect angle of a man-made target produce a BRDF attenuation as compared to laboratory experiments. More generally, the model simply relaxes the unitary constraint, sometimes improperly assumed on the abundances by the replacement model. We developed two GLRTs for the model at hand, namely the one-step and two-steps

GLRT. Numerical simulations showed that these solutions are attractive as soon as the target signature attenuation reaches 30%, compared to solutions exploiting the unitary constraint. Moreover a real data experiment showed that considering the modified replacement model and the proposed solutions is worthy of interest for real applications.

[1] D. G. Manolakis, R. B. Lockwood, T. W. Cooley, Hyperspectral Imaging Remote Sensing, Cambridge University Press, 2016.

[2] E. K. Hege, D. O'Connell, W. Johnson, S. Basty, E. L. Dereniak, Hyperspectral imaging for astronomy and space surveillance, in: Proc. SPIE, vol. 5159, 2004.

[3] S. Michel, P. Gamet, M. J. Lefevre-Fonollosa, HYPXIM A hyperspectral satellite defined for science, security and defence users, in: Proceesings 3rd Workshop on Hyperspectral Image and Signal Processing: Evolution in Remote Sensing (WHISPERS), 2011.

[4] H. Kwon, N. Nasrabadi, Kernel RX-algorithm: a nonlinear anomaly detector for hyperspectral imagery, IEEE Transactions Geoscience Remote Sensing 43 (2) (2005) 388 – 397.

[5] E. M. Winter, M. Miller, C. Simi, A. Hill, T. Williams, D. Hampton, M. Wood, J. Zadnick, M. Sviland, Mine detection experiments using hyperspectral sensors, in: SPIE Int. Soc. Opt. Eng., Orlando, FL, United States, 2004.

[6] C. Funk, J. Theiler, D. Roberts, C. Borel, Clustering to improve matched filter detection of weak gas plumes in hyperspectral thermal imagery, IEEE Transactions Geoscience Remote Sensing 39 (7) (2001) 1410 – 1420.

[7] D.-W. Sun, Hyperspectral Imaging for Food Quality Analysis and Control, Elsevier, 2010.

[8] R. Koprowski, Processing of Hyperspectral Medical Images, Applications in Dermatology Using Matlab, Springer International Publishing, 2017.

[9] D. Manolakis, G. Shaw, Detection algorithms for hyperspectral imaging applications, IEEE Signal Processing Magazine (2002) 29–43.

[10] E. Kelly, An Adaptive Detection Algorithm, IEEE Transactions Aerospace Electronic Systems 22 (2) (1986) 115–127.

[11] C. Chang, Orthogonal subspace projection (OSP) revisited: A comprehensive study and analysis, IEEE Transactions Geoscience Remote Sensing 43 (3) (2005) 502–518.

[12] S. Kraut, L. L. Scharf, L. T. McWhorter, Adaptive subspace detectors, IEEE Transactions Signal Processing 49 (1) (2001) 1 – 16.

[13] A. Schaum, A. Stocker, Spectrally-Selective Target Detection, in: Proceedings of ISSSR, vol. 12, 2015–2018, 1997.

[14] F. Vincent, O. Besson, Generalized Likelihood Ratio Test for Subpixel Target Detection in Hyperspectral Imaging, IEEE Transactions Geoscience Remote Sensing Under Review.

[15] W. Verhoef, H. Bach, Simulation of hyperspectral and directional radiance images using coupled biophysical and atmospheric radiative transfer models, Elsevier, Remote Sensing of Environment 87 (2003) 2341.

[16] V. Roy, Hybrid algorithm for hyperspectral target detection, in: Proc. SPIE 7695, Algorithms and Technologies for Multispectral, Hyperspectral, and Ultraspectral Imagery XVI, 769522, 2010.

[17] D. Manolakis, R. Lockwood, T. Cooley, J. Jacobson, Is There a Best Hyperspectral Detection Algorithm?, in: Proc. of SPIE, vol. 7334, 2009.

[18] N. Acito, S. Matteoli, A. Rossi, M. Diani, G. Corsini, Hyperspectral Airborne Viareggio 2013 Trial Data Collection for Detection Algorithm Assessment, IEEE Journal of Selected Topics in Applied Earth Observations and Remote Sensing 9 (6) (2016) 2356 – 2376.

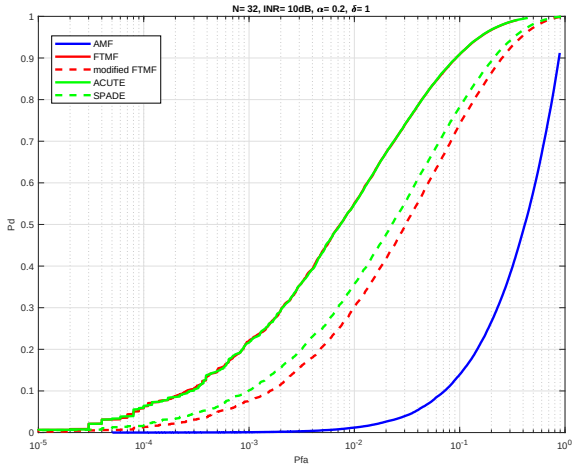

Figure 1: ROC from 10^5 Monte-Carlo simulations for an INR of $-10dB$, $N = 32$, $K = 10N$, $\alpha = 0.2$ and $\delta = 1$

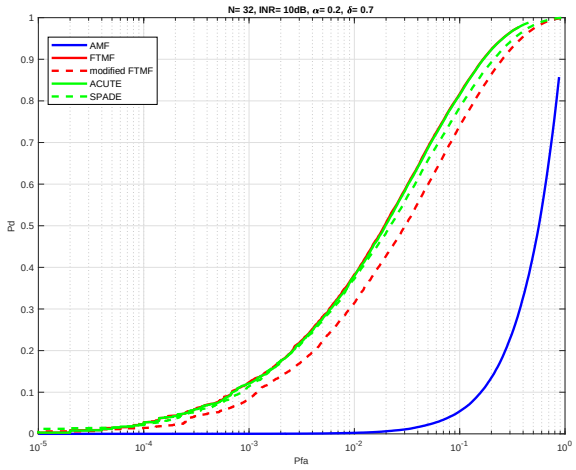

Figure 2: ROC from 10^5 Monte-Carlo simulations for an INR of $-10dB$, $N = 32$, $K = 10N$, $\alpha = 0.2$ and $\delta = 0.7$

Table 1: False Alarms Numbers

Target	**AMF**	**FTMF**	**Modified FTMF**	**ACUTE**	**SPADE**
V5	7	1	7	0	0
V6	147	284	167	133	89

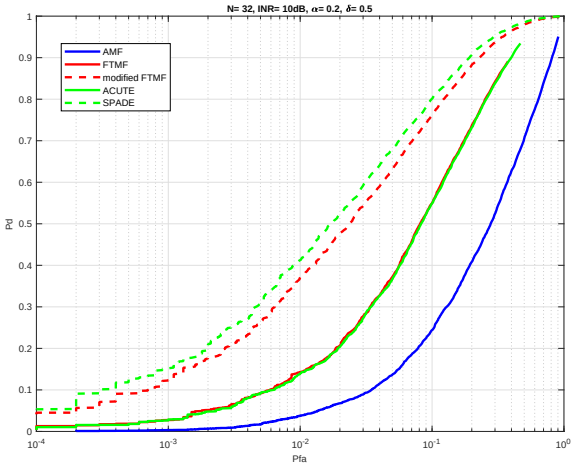

Figure 3: ROC from 10^5 Monte-Carlo simulations for an INR of $-10dB$, $N = 32$, $K = 10N$, $\alpha = 0.2$ and $\delta = 0.5$

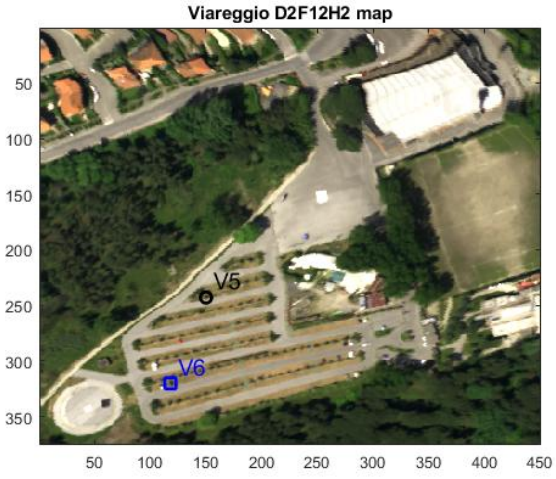

Figure 4: Complete RGB view of the scene